

Interactions of Carbon Dioxide with Liquid Fluorocarbons

Margarida F. Costa Gomes and Agílio A. H. Pádua*

Laboratoire de Thermodynamique des Solutions et des Polymères, CNRS UMR 6003 and Université Blaise Pascal Clermont-Ferrand, 63177 Aubière, France

Received: June 11, 2003; In Final Form: September 29, 2003

The interactions of carbon dioxide with liquid fluorinated and hydrogenated hydrocarbons, perfluoro-*n*-hexane and *n*-hexane, are investigated by computer simulation. Conformational and structural properties of the liquid phases were obtained applying the molecular dynamics method using flexible, all-atom force fields containing electrostatic charges. It was verified that spontaneous cavities are larger and more easily formed in the fluorocarbon, corresponding to smaller free energies of cavity formation, than in the equivalent hydrocarbon. These facts do not explain the high solubility of carbon dioxide compared to that of other gases, a behavior resulting from differences in solute–solvent interactions. The chemical potential at infinite dilution and the solubility of carbon dioxide and oxygen in the solvents were determined from the simulation runs by the method of test-particle insertion. It is demonstrated that electrostatics play a minor role in the forces between carbon dioxide and both alkanes and perfluoroalkanes, which are mainly governed by dispersion terms. No evidence of a particular affinity of carbon dioxide for perfluorinated liquids was found either from the results of the present or from analysis of literature data on gas solubility.

Introduction

Fluorinated fluid phases have been attracting attention from different fields of application: in organic synthesis and separation methods, because fluorinated species are nontoxic and immiscible with both hydrocarbons and water,¹ and in biomedical applications as gas carriers in vivo or ultrasound contrast agents.² Fluorinated molecules also provide a means to improve the solubility of chemicals in supercritical³ reaction or extraction media.⁴ Despite the growing number of applications, the understanding of key phenomena governing the solvation properties involving fluorinated species is still incomplete, and seemingly contradictory observations remain to be explained.

The purpose of the present work is to clarify the molecular mechanisms underlying the solubility of small molecules, like carbon dioxide and oxygen, in liquid fluorocarbons. Namely to elucidate the enhanced mutual solubility of CO₂ and fluorinated molecules and to clarify some ambiguities concerning the existence of specific CO₂–fluorocarbon interactions. To achieve this, two aspects are appreciated here: structural details of pure fluorocarbon and hydrocarbon liquid phases, and the nature of the solute–solvent interactions. This decomposition follows the spirit of scaled particle theory⁵ which has contributed to explain, at a molecular level, solvation properties of water such as the hydrophobic effect.^{6,7}

In the literature, contradictory results have been reported, both theoretical and experimental, concerning the nature of the molecular forces between CO₂ and fluorinated compounds. On the experimental side, one high-pressure NMR study⁸ suggested the existence of specific attractive interactions (with *n*-hexane, perfluoro-*n*-hexane, and 1,1-dihydroperfluorooctylpropionate), whereas a previous infrared study⁹ had described more repulsive interactions between carbon dioxide and perfluoroethane and perfluorobutanol than with their hydrogenated counterparts.

More recently, other high-pressure NMR studies^{10,11} found no evidence of the existence of specific interactions between CO₂ and fluorocarbons (different fluoromethanes and perfluorobenzene).

On the theoretical side, *ab initio* calculations at Hartree–Fock/6-31G(d) level attributed a larger binding energy to the pair CO₂–perfluoroethane than to CO₂–ethane, leading the authors to postulate a stronger electrostatic interaction with the fluorinated molecule.¹² Opposite results were obtained at the Möller–Plesset level of theory using a larger basis set (cc-pVTZ) and correcting for basis set superposition errors.¹³ This time, no evidence for enhanced interactions between CO₂ and perfluoroethane was found and, if anything, small hydrocarbons seemed to exhibit even stronger binding with the gas than the corresponding fluorocarbons.¹³ Neither of these quantum calculations can totally clarify the nature of the interactions between carbon dioxide and perfluorocarbon molecules in solution. The properties of liquid mixtures are governed by solute–solute, solvent–solvent, and solute–solvent interactions and by entropic as well as enthalpic terms; therefore, theoretical studies uniquely of solute–solvent energetics in the gas phase provide only partial information.

A molecular simulation study has been reported in which vapor–liquid equilibrium in CO₂–perfluorohexane and CO₂–hexane mixtures is modeled using united-atom descriptions of hexane and perfluorohexane,¹⁴ therefore, without explicit Coulombic interactions between CO₂ and hexane or perfluorohexane. In that study, simulations are compared to experimental vapor–liquid equilibrium data^{9,15} which had shown the increased miscibility between perfluorohexane and CO₂. The results of a pure prediction (assuming Lorentz–Berthelot combining rules for the unlike interactions) were in relative good agreement with the experiment: mole fractions of carbon dioxide in phases rich in hexane and perfluorohexane were overestimated by about 10% and 13%, respectively. The authors concluded that addition of electrostatic interactions or explicit fluorine atoms in the

* To whom correspondence should be addressed. E-mail: agilio.padua@univ.bpclermont.fr.

TABLE 1: Parameters of the Explicit-atom Intermolecular Potentials

	$\sigma/\text{\AA}$	$\epsilon/\text{kJ mol}^{-1}$	q/e
C ₆ H ₁₄			
C	3.500	0.2761	-0.12, -0.18
H	2.500	0.1255	+0.06
C ₆ F ₁₄			
C	3.500	0.2761	+0.24, +0.36
F	2.950	0.2218	-0.12
O ₂			
O	3.030	0.4016	0
CO ₂			
C	2.757	0.2339	+0.6512
O	3.033	0.6694	-0.3256

molecular models for perfluorocarbons might improve their results and reproduce more accurately the experimental values.

This is probably the best approach to study the dependence of macroscopic thermodynamic properties on the underlying molecular interactions. Simulation can, in addition, elucidate microscopic structural details which are difficult to access experimentally. The accuracy of the simulation results depends on the reliability of the force-field model. This can be checked by comparison of the simulation results to measurable properties such as solubility, which seems adequate for this purpose because it probes directly the chemical potential of the solute, allows the derivation of several thermodynamic functions of solvation, and, in the case of the systems of interest here, has been rigorously measured by several authors. Although the present work is focused on the solubility of gaseous CO₂ in hydrocarbons and perfluorocarbons, the similarity of the interaction pairs involved establishes a connection to the field of supercritical fluids.

In the present study, computer simulations of perfluoro-*n*-hexane and of *n*-hexane were performed using all-atom force fields. These recently proposed models for long-chain perfluoroalkanes¹⁶ (containing three or more carbon atoms) provide a more detailed, and probably more accurate, molecular description than previous attempts based on the united-atom framework.^{17,18} The new OPLS-AA model adds explicit sites and partial charges to individual atoms in addition to a finer representation of the conformational energetics. These features enable an investigation by simulation of the structural details of the liquid fluorocarbon and hydrocarbon phases and of the role of electrostatics in the interactions of CO₂ with those liquids.

Molecular Simulations

Simulations were performed using the molecular dynamics technique, implemented in the DL POLY¹⁹ computer code. The molecules of *n*-hexane and perfluoro-*n*-hexane were represented by flexible force fields in which all atoms are considered explicitly. Parameters for both solvents were taken from the OPLS-AA force field for alkanes²⁰ and for perfluoroalkanes.¹⁶ These models contain a fully flexible description of the molecular skeleton and Lennard-Jones interaction sites plus point charges placed in all of the atom sites. The intermolecular parameters are summarized in Table 1. Within the same molecule, atoms separated by more than three covalent bonds also interact through the nonbonded Lennard-Jones plus Coulomb forces scaled by a factor of 0.5. In the present simulations, the C–H bonds were replaced by rigid constraints, allowing the simulations to be performed using a time step of 1 fs without registering drifts of the total energy in the microcanonical ensemble. Spherical cutoffs of 12 Å were adopted for the nonbonded interactions, and the Ewald summation method was used for the long-range electrostatic terms, with a number of

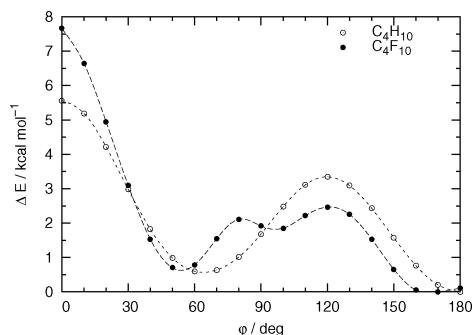


Figure 1. Torsion energy profiles corresponding to rotation around the central C–C–C bond in *n*-butane and in perfluoro-*n*-butane. Energies obtained from relaxed dihedral angle scans using a quantum chemistry software package²¹ at the MP2/cc-pVTZ(-f)/HF/6-31G(d) level.

reciprocal cell vectors of 6 in the case of the alkane and 8 or 9 for the perfluoroalkane. Periodic cubic boxes containing 200 molecules of both substances were simulated at 1 bar and at 200, 300, and 400 K using Nosé-Hoover barostat and thermostat, in runs of 100 ps after equilibration. Samples of 1000 configurations were stored for further treatment.

Liquid-Phase Structure of the Pure Solvents. One important feature distinguishing *n*-alkanes from perfluoro-*n*-alkanes is the torsion energy profile around a central C–C–C bond. In alkanes, an absolute minimum of potential energy is found for a torsional angle of 180°, corresponding to the trans conformer, and a relative minimum is found at 60°, corresponding to gauche conformations.²⁰ The picture for perfluoro-*n*-alkanes is different:¹⁶ the occurrence of absolute minima which do not correspond to the trans but to anti conformers, and these minima are located at about 170°, on both sides of the staggered form. Also the eclipsed barrier to internal rotation is higher than that of the alkanes. These features are illustrated in Figure 1 for butane and perfluorobutane. The energy profiles were calculated ab initio at the MP2/cc-pVTZ(-f)/HF/6-31G(d) level using a quantum chemistry software package.²¹ The molecular geometries were first optimized at the HF/6-31G(d) level after which single-point energy calculations were performed at the MP2 level using a larger basis set (the cc-pVTZ basis set of Dunning²² after removal of the f functions). The OPLS-AA force fields used in the computer simulations reproduce correctly these torsion energy profiles.^{20,16}

Molecular dynamics simulations of *n*-hexane and perfluoro-*n*-hexane in the liquid state show that most of the dihedral angles in the carbon skeleton of *n*-alkanes adopt values close to 180° with occasional occurrence gauche defects. The population of these gauche defects depends on temperature as can be seen in Figure 2. When compared to the corresponding perfluoro-*n*-alkane, whose results are shown in Figure 3, the population of gauche defects is smaller in the latter case, an indication of a more rigid molecular backbone. This suggests that cavities present naturally in the liquid phase may be larger in fluoroalkanes than in alkanes.

The nature of the cavities spontaneously present in both liquids was studied by calculating the distribution of cavity sizes and the free energy of cavity formation from the computer simulations. We chose to calculate the free energies of cavity formation by testing the probability of inserting hard spheres using Widom's method:^{6,23,24}

$$\mu_{\text{cav}}(r) = -kT \ln \frac{\langle V \exp(-u_{\text{HS}}(r)/kT) \rangle_{NpT}}{\langle V \rangle} \quad (1)$$

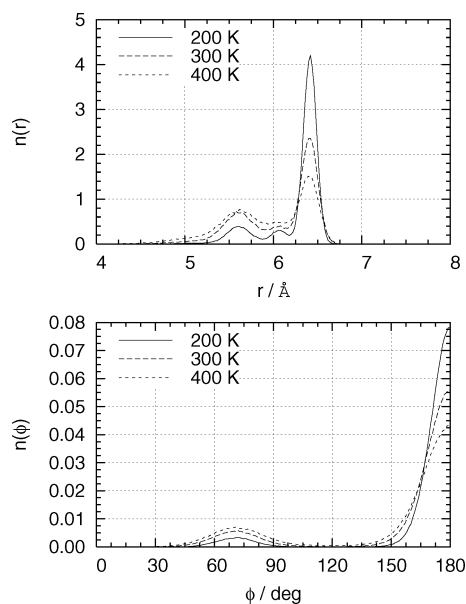


Figure 2. Distribution of end-to-end distances and C–C–C dihedral angles in liquid *n*-hexane. Results obtained from molecular dynamics simulation of 200 molecules described by the OPLS all-atom force field at several temperatures.

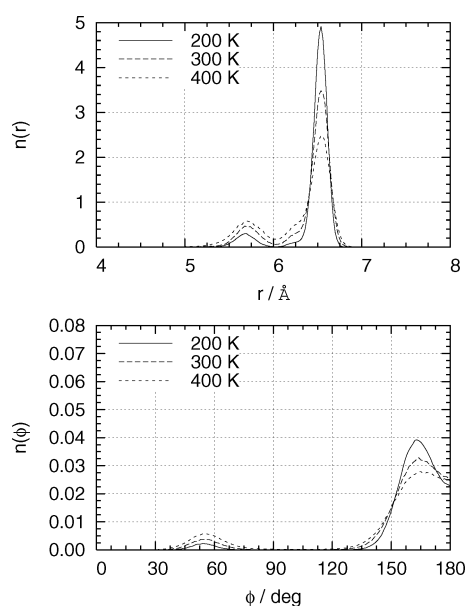


Figure 3. Distribution of end-to-end distances and C–C–C dihedral angles in perfluoro-*n*-hexane. Results obtained from molecular dynamics simulation of 200 molecules described by the OPLS all-atom force field at several temperatures.

where V is the volume of the simulation box and $\exp(-u_{\text{HS}}(r)/kT)$ is either 1 or 0 if a cavity of radius up to r exists ($u_{\text{HS}} = 0$) or else overlaps a solvent molecule ($u_{\text{HS}} = +\infty$) at a trial location, respectively. The Lennard-Jones diameters σ of the atoms in the solvent molecules were considered as overlap condition with the hard cavity. The brackets $\langle \dots \rangle$ denote isothermal–isobaric ensemble averages over the stored configurations. In each of the 1000 solvent configurations stored, 60 000 insertions were tried at random locations.

The distribution of cavity sizes is represented in Figure 4. It demonstrates that the population of cavities of a given size is always larger in the fluorinated alkane than in its hydrocarbon counterpart. Furthermore, in the temperature range covered, forming a cavity in the fluorinated liquid always requires less

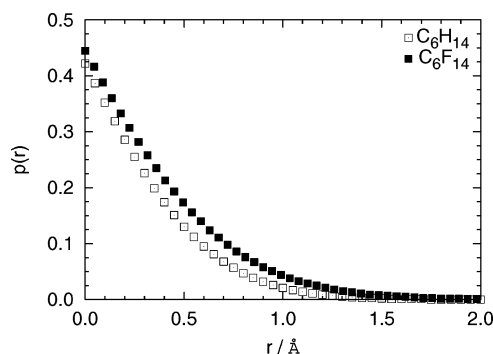


Figure 4. Acceptance probability that a sphere of radius r placed at random in the system does not overlap any of the molecules of *n*-hexane or of perfluoro-*n*-hexane at 300 K.

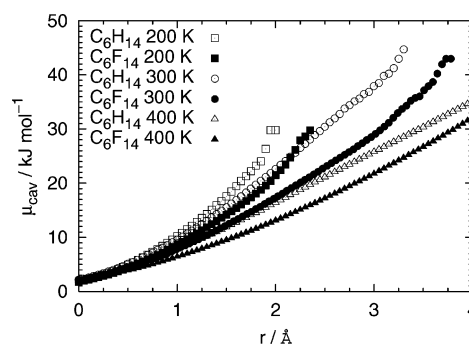


Figure 5. Free energy of cavity formation in *n*-hexane and perfluoro-*n*-hexane determined by test-particle insertion of hard spheres.

work than in the hydrogenated species, as shown by the calculated free energies of cavity formation plotted in Figure 5.

From these results, it would be expected that lower molecular volume solutes should in general be more soluble. This is not the case when the solubility of CO_2 is compared to that of oxygen or with other gases such as nitrogen or argon, for example,^{25,26,27} meaning that solute–solvent interactions determine the enhanced solubility of CO_2 .

Gas–Solvent Interactions. To elucidate the role of the gas–solvent interactions, the solubilities of O_2 and CO_2 were calculated from the simulation results using the method of test-particle insertion.²⁸ The interaction potential models used for the solute gases are of the type Lennard-Jones plus charges: the rigid two-center model of Miyano²⁹ for the O_2 molecule and the EPM model of Harris and Yung³⁰ for CO_2 . The latter incorporates partial charges and may include a flexible bond angle, but in the present work, the CO_2 molecule was considered to be rigid. The parameters describing both solutes are summarized in Table 1. Interactions between the gaseous solutes and the fluorinated or hydrogenated solvents were assumed to obey geometric combining rules for the Lennard-Jones parameters, and therefore, no unlike interaction parameters were introduced. These choices proved appropriate to model the solubility of O_2 and CO_2 in different hydrocarbon and fluoro-carbon liquids.^{31,32}

The residual chemical potential of the solute gases at infinite dilution was calculated by trial insertions of the solute molecule, at random positions and orientations, in each of the solvent snapshots previously stored. The insertions were tried 90 000 times per configuration of solvent. The residual chemical potential of the solute, μ_2^r , is the difference between the chemical potential of the solute in the solution and that of the solute in the ideal gas state at the same temperature and density. This corresponds to the same free energy difference as that of

TABLE 2: Residual Chemical Potential at Infinite Dilution and Solubility of Oxygen and Carbon Dioxide in *n*-Hexane and in Perfluoro-*n*-hexane^a

<i>T</i> /K	$\rho_1/\text{mol L}^{-1}$	$\mu_2^{\text{r}\infty}/\text{kJ mol}^{-1}$	$10^{-3}x_2$	$\rho_1/\text{mol L}^{-1}$	$\mu_2^{\text{r}\infty}/\text{kJ mol}^{-1}$	$10^{-3}x_2$
O ₂						
		C ₆ H ₁₄			C ₆ F ₁₄	
200	8.73 ± 0.01	0.28 ± 0.11	5.9 ± 0.4	5.77 ± 0.01	0.06 ± 0.15	10 ± 1
300	7.53 ± 0.01	1.46 ± 0.04	3.0 ± 0.1	4.91 ± 0.02	1.07 ± 0.07	5.4 ± 0.1
400	6.11 ± 0.04	1.54 ± 0.06	3.1 ± 0.1	3.91 ± 0.04	1.40 ± 0.08	5.1 ± 0.1
CO ₂						
		C ₆ H ₁₄			C ₆ F ₁₄	
200	8.73 ± 0.01	-5.35 ± 0.29	174 ± 30	5.77 ± 0.01	-5.13 ± 0.28	231 ± 39
300	7.53 ± 0.01	-2.80 ± 0.06	16.6 ± 0.4	4.91 ± 0.02	-2.69 ± 0.08	24.3 ± 0.8
400	6.11 ± 0.04	-1.54 ± 0.04	7.9 ± 0.1	3.91 ± 0.04	-1.21 ± 0.06	11.2 ± 0.2
CO ₂ (no electrostatics)						
		C ₆ H ₁₄			C ₆ F ₁₄	
200	8.73 ± 0.01	-5.32 ± 0.28	171 ± 29	5.77 ± 0.01	-4.86 ± 0.29	196 ± 34
300	7.53 ± 0.01	-2.80 ± 0.06	16.6 ± 0.4	4.91 ± 0.02	-2.48 ± 0.08	22.4 ± 0.7
400	6.11 ± 0.04	-1.57 ± 0.04	8.0 ± 0.1	3.91 ± 0.04	-1.07 ± 0.06	10.7 ± 0.2

^a Results obtained from the test-particle insertion method after simulation of the pure liquids.

TABLE 3: Experimental Solubilities of Gases ($10^{-3}x_2$) at 298 K in Various Hydrocarbon and Fluorocarbon Solvents

	O ₂	CO ₂	CO
<i>n</i> -C ₆ H ₁₄	1.99[32]		
<i>n</i> -C ₇ H ₁₆	2.04[38]		
<i>n</i> -C ₈ H ₁₈	2.05[38]	12.6[25]	1.71[25]
C ₆ H ₆	0.815[26]	9.70[26]	0.663[26]
<i>n</i> -C ₆ F ₁₄	4.23[32]		
<i>n</i> -C ₇ F ₁₆	5.22[27]		
<i>n</i> -C ₈ F ₁₈	5.34[39]		
C ₆ F ₆	2.41[26]	22.0[26]	2.12[26]
$x(\text{C}_6\text{F}_{14})/x(\text{C}_6\text{H}_{14})$	2.13		
$x(\text{C}_7\text{F}_{16})/x(\text{C}_7\text{H}_{16})$	2.56	1.73[27]	2.24[27]
$x(\text{C}_8\text{F}_{18})/x(\text{C}_8\text{H}_{18})$	2.60		
$x(\text{C}_6\text{F}_6)/x(\text{C}_6\text{H}_6)$	2.96	2.27	3.20

the solvation process.^{33,34} For simulations at constant NpT , μ_2^{r} is given by

$$\mu_2^{\text{r}} = -kT \ln \frac{\langle V \exp(-u_{\text{TP}}/kT) \rangle_{NpT}}{\langle V \rangle} \quad (2)$$

where u_{TP} is the interaction energy of the test particle with a molecular configuration of the solution. Henry's law coefficients, K_{H} , were calculated from the residual chemical potential at infinite dilution, since the stored configurations describe the pure solvents

$$K_{\text{H}}(p, T) = \rho_1 kT \exp\left(\frac{\mu_2^{\text{r}\infty}}{kT}\right) \quad (3)$$

where ρ_1 is the density of the pure solvent. From these values, the calculation of the mole fraction of dissolved gas under a partial pressure of 1 atm, which is a usual way of conveying the solubility, is immediate.³⁵

The residual chemical potentials and mole fraction solubilities of O₂ and CO₂ calculated from simulation are listed in Table 2, accompanied by the statistical uncertainties obtained following to the block-average procedure.³⁶ As expected, the solubility of CO₂ is substantially superior to that of oxygen in both solvents but not particularly in the fluorinated liquid. Remarkably, the solubility of O₂ in the two liquids differs more in relative terms than that of CO₂. This behavior observed in the simulation results is validated by comparison with experimental data reported in the literature which are collected in Table 3. A direct comparison between our simulations and the experimental data is possible for O₂ in both C₆H₁₄ and C₆F₁₄. In absolute

terms, the values are in reasonable agreement, showing levels of accuracy common in this kind of totally predictive calculation (no unlike interaction parameters were adjusted). The ratio of the solubility in the two solvents, 2.13 experimentally, is well reproduced by the simulations with a result of 1.8.

To determine the role of electrostatics in the interaction between CO₂ and both liquids, these calculations were repeated taking the same model for the CO₂ molecule but this time excluding partial charges. It was observed that the residual chemical potentials, or the solubilities, obtained were very close to those calculated using the full model, taking into account the statistical uncertainties. This demonstrates the minor role played by the electrostatic terms.

This fact is confirmed by the comparison of the solubilities of O₂ and CO₂ to those of carbon monoxide, where a small dipole moment is present. It is found that CO behaves much like O₂, reinforcing the idea that the key factor in the present solute-solvent interactions is not related to electrostatic terms but to dispersion forces. This conclusion is sustained by the comparison of the polarizabilities:³⁷ the value for CO ($\alpha = 1.95 \text{ \AA}^3$) is closer to that for O₂ ($\alpha = 1.60 \text{ \AA}^3$) than to the one for CO₂ ($\alpha = 2.65 \text{ \AA}^3$).

The Lennard-Jones parameters of the oxygen atoms in CO₂ correspond to a deeper attractive well than that found with the parameters of O₂. Curiously, the values for the carbon atom correspond to a shallower attractive well than that found in alkanes²⁰ ($\sigma = 3.50 \text{ \AA}$, $\epsilon = 0.276 \text{ kJ mol}^{-1}$). This translates the fact that the models used render correctly the enhanced electron density around the oxygen atoms in CO₂, and the consequent decrease in electron density around the carbon atom, which are the origin of the quadrupole moment. This quadrupole moment is not, however, the direct cause of the stronger attractions to nonpolar liquids.

Conclusions

Structural details of the liquid *n*-hexane and perfluoro-*n*-hexane phases were investigated by comparing the torsion energy profiles around the carbon skeletons and by studying the nature of the spontaneous cavities (distribution of cavity sizes and free energies of cavity formation) present in the pure liquids. This analysis permitted the molecular interpretation of the experimental fact that fluorocarbon solvents always dissolve larger amounts of a particular gas than the equivalent hydrocarbons⁴⁰ but fails to explain the differences between the solubility of oxygen and carbon dioxide in a fluorinated liquid.

It was shown that liquid fluorocarbon phases present larger cavities of a given size and that the free energy of cavity formation is always smaller than for the equivalent hydrocarbon. These facts do not, however, explain the differences in the relative solubilities of carbon dioxide and oxygen (the first having a larger molecular volume) which are in fact determined by energetics of solute–solvent interaction.

The gas-solvent interactions were also studied by computer simulation through the calculation of the chemical potential of carbon dioxide and oxygen in *n*-hexane and perfluoro-*n*-hexane. The results clarify the nature of the molecular interactions between carbon dioxide and fluorinated solvents. It has been demonstrated by molecular simulation that electrostatic terms play a minor role in the interactions between carbon dioxide and both alkanes and perfluoroalkanes. The stronger interactions of carbon dioxide with nonpolar solvents should be attributed to dispersion forces.

Furthermore, it was verified by an analysis of literature data on the solubilities of other gases, that carbon dioxide does not have a preferential affinity for perfluorinated liquids when compared to their hydrogenated counterparts. The present simulations are in total agreement with this fact.

Acknowledgment. This work benefitted from allocation of computer resources at the Institut du Développement et des Ressources en Informatique Scientifique (IDRIS) du Centre National de la Recherche Scientifique, and of the Centre Informatique National de l'Enseignement Supérieur (CINES), France.

References and Notes

- (1) Horvath, I. T.; Rabai, J. *Science* **1994**, 266, 72.
- (2) Riess, J. G. *Chem. Rev.* **2001**, 101, 2797.
- (3) Eckert, C. A.; Knutson, B. L.; Debenedetti, P. G. *Nature* **1996**, 383, 313.
- (4) Johnston, K. P.; Harrison, K. L.; Clarke, M. J.; Howdle, S. M.; Heitz, M. P.; Bright, F. V.; Carlier, C.; Randolph, T. W. *Science* **1996**, 271, 624.
- (5) Pierotti, R. A. *J. Phys. Chem.* **1965**, 69, 281.
- (6) Pratt, L. R.; Pohorille, A. *Proc. Natl. Acad. Sci.* **1992**, 89, 2995.
- (7) Southall, N. T.; Dill, K. A.; Haymet, A. D. *J. Phys. Chem. B* **2002**, 106, 521.
- (8) Dardin, A.; DeSimone, J.; Samulki, E. T. *J. Phys. Chem. B* **1998**, 102, 1775.
- (9) Yee, G. G.; Fulton, J. L.; Smith, R. D. *J. Phys. Chem.* **1992**, 96, 6172.
- (10) Yonker, C. R. *J. Phys. Chem. A* **2000**, 104, 685.
- (11) Yonker, C. R.; Palmer, B. J. *J. Phys. Chem. A* **2001**, 105, 308.
- (12) Cece, A.; Jureller, S. H.; Kerscher, J. L.; Moschner, K. F. *J. Phys. Chem.* **1996**, 100, 7435.
- (13) Diep, P.; Jordan, K. D.; Johnson, J. K.; Beckman, E. J. *J. Phys. Chem. A* **1998**, 102, 2231.
- (14) Cui, S. T.; Cochran, H. D.; Cummings, P. T. *J. Phys. Chem. B* **1999**, 103, 4485.
- (15) Iezzi, A.; Bendale, P.; Enick, R. M.; Turberg, M.; Brady, J. *Fluid Phase Equilibria* **1989**, 52, 307.
- (16) Watkins, E. K.; Jorgensen, W. L. *J. Phys. Chem. A* **2001**, 105, 4118.
- (17) Shin, S.; Collazo, N.; Rice, S. A. *J. Chem. Phys.* **1992**, 96, 1352.
- (18) Cui, S. T.; Siepmann, J. I.; Cochran, H. D.; Cummings, P. T. *Fluid Phase Equilibria* **1998**, 146, 51.
- (19) Smith, W.; Forester, T. R., *The DL_POLY package of molecular simulation routines, version 2.12*, The Council for the Central Laboratory of Research Councils; Daresbury Laboratory: Warrington, U.K., 1999.
- (20) Jorgensen, W. L.; Maxwell, D. S.; Tirado-Rives, J. *J. Am. Chem. Soc.* **1996**, 118, 11225.
- (21) Frisch, M. J.; Trucks, G. W.; Schlegel, H. B.; Scuseria, G. E.; Robb, M. A.; Cheeseman, J. R.; Zakrzewski, V. G.; Montgomery, J. A., Jr.; Stratmann, R. E.; Burant, J. C.; Dapprich, S.; Millam, J. M.; Daniels, A. D.; Kudin, K. N.; Strain, M. C.; Farkas, O.; Tomasi, J.; Barone, V.; Cossi, M.; Cammi, R.; Mennucci, B.; Pomelli, C.; Adamo, C.; Clifford, S.; Ochterski, J.; Petersson, G. A.; Ayala, P. Y.; Cui, Q.; Morokuma, K.; Malick, D. K.; Rabuck, A. D.; Raghavachari, K.; Foresman, J. B.; Cioslowski, J.; Ortiz, J. V.; Stefanov, B. B.; Liu, G.; Liashenko, A.; Piskorz, P.; Komaromi, I.; Gomperts, R.; Martin, R. L.; Fox, D. J.; Keith, T.; Al-Laham, M. A.; Peng, C. Y.; Nanayakkara, A.; Gonzalez, C.; Challacombe, M.; Gill, P. M. W.; Johnson, B. G.; Chen, W.; Wong, M. W.; Andres, J. L.; Head-Gordon, M.; Replogle, E. S.; Pople, J. A. *Gaussian 98*, revision A.9; Gaussian, Inc.: Pittsburgh, PA, 1998.
- (22) Dunning, T. H., Jr. *J. Chem. Phys.* **1989**, 90, 1007.
- (23) Prévost, M.; Oliveira, I. T.; Kocher, J.-P.; Wodak, S. J. *J. Phys. Chem.* **1996**, 100, 2738.
- (24) Ikeguchi, M.; Shimizu, S.; Nakamura, S.; Shimitzu, K. *J. Phys. Chem. B* **1998**, 102, 5891.
- (25) Wilcock, R. J.; Battino, R.; Danforth, W. F.; Wilhelm, E. *J. Chem. Thermodyn.* **1978**, 10, 817.
- (26) Evans, F. D.; Battino, R. *J. Chem. Thermodyn.* **1971**, 3, 753.
- (27) Wilhelm, E.; Battino, R. *J. Chem. Thermodyn.* **1971**, 3, 761.
- (28) Widom, B. *J. Chem. Phys.* **1963**, 39, 2908.
- (29) Miyano, Y. *Fluid Phase Equilib.* **1999**, 158–160, 29.
- (30) Harris, J. G.; Yung, K. H. *J. Phys. Chem.* **1995**, 99, 12021.
- (31) Pádua, A. A. H. *J. Phys. Chem. A* **2002**, 106, 10116.
- (32) Dias, A. M. A.; Bonifácio, R. P.; Marrucho, I. M.; Pádua, A. A. H.; Costa Gomes, M. F. *Phys. Chem. Chem. Phys.* **2003**, 5, 543.
- (33) Ben-Naim, A. *Water and aqueous solutions. Introduction to a molecular theory*; Plenum Press: New York, 1974.
- (34) Ben-Naim, A.; Marcy, Y. *J. Chem. Phys.* **1984**, 81, 2016.
- (35) Smith, J. M.; Ness, H. C. V.; Abbott, M. M., *Introduction to Chemical Engineering Thermodynamics*, 5th ed.; McGraw-Hill: New York, 1996.
- (36) Allen, M. P.; Tildesley, D. J., *Computer Simulation of Liquids*; Oxford University Press: Oxford, U.K., 1987.
- (37) Hirschfelder, J.; Curtiss, C.; Bird, R., *Molecular Theory of Gases and Liquids*; Wiley, New York, 1954.
- (38) Hesse, P. J.; Battino, R.; Scharlin, P.; Wilhelm, E. *J. Chem. Eng. Data* **1996**, 41, 195.
- (39) Lawson, D. D.; Moacanin, J.; Sherer, K. V.; Terranova, T. F.; Ingham, J. D. *J. Fluorine Chem.* **1978**, 12, 221.
- (40) Hildebrand, J. H.; Prausnitz, J. M.; Scott, R. L., *Regular and Related Solutions*; Van Nostrand Reinhold Co.: New York, 1970.